OXFORD

Cerebral Cortex, 2023, **33**, 10736–10749
https://doi.org/10.1093/cercor/bhad309
Advance access publication date 13 September 2023
Original Article

Characterizing brain stage-dependent pupil dynamics based on lateral hypothalamic activity

Kengo Takahashi [1,2,3], Filip Sobczak [1], Patricia Pais-Roldán [4], Xin Yu [5,*]

[1]High-Field Magnetic Resonance Department, Max Planck Institute for Biological Cybernetics, 72076 Tübingen, Germany,
[2]Graduate Training Centre of Neuroscience, International Max Planck Research School (IMPRS), University of Tübingen, 72076 Tübingen, Germany,
[3]Cognitive and Systems Neuroscience Group, Swammerdam Institute for Life Sciences, Faculty of Science, University of Amsterdam, 1098XH Amsterdam, The Netherlands,
[4]Medical Imaging Physics, Institute of Neuroscience and Medicine (INM-4), Forschungszentrum Jülich, 52425 Jülich, Germany,
[5]Athinoula A. Martinos Center for Biomedical Imaging, Massachusetts General Hospital, Harvard Medical School, Charlestown, MA 02129, United States

*Corresponding author: 149 13th. Street, Charlestown, MA 02129, United States. Email: xyu9@mgh.harvard.edu

Pupil dynamics presents varied correlation features with brain activity under different vigilant levels. The modulation of brain dynamic stages can arise from the lateral hypothalamus (LH), where diverse neuronal cell types contribute to arousal regulation in opposite directions via the anterior cingulate cortex (ACC). However, the relationship of the LH and pupil dynamics has seldom been investigated. Here, we performed local field potential (LFP) recordings at the LH and ACC, and whole-brain fMRI with simultaneous fiber photometry Ca^{2+} recording in the ACC, to evaluate their correlation with brain state-dependent pupil dynamics. Both LFP and functional magnetic resonance imaging (fMRI) data showed various correlations to pupil dynamics across trials that span negative, null, and positive correlation values, demonstrating brain state-dependent coupling features. Our results indicate that the correlation of pupil dynamics with ACC LFP and whole-brain fMRI signals depends on LH activity, suggesting a role of the latter in brain dynamic stage regulation.

Key words: lateral hypothalamus; anterior cingulate cortex; multimodal resting-state fMRI; brain dynamic stages; pupillometry.

Introduction

Brain state fluctuation, as a fundamental feature of animal brain physiology, is related to arousal regulation during wakefulness, sleep, or under anesthesia (Saper et al. 2001; Brown et al. 2010; McGinley et al. 2015). A transition of brain dynamic stages can arise between two radically different sub-states such as REM and NREM sleep but also between more complex sub-states such as those emerging under anesthesia (Brown et al. 2010; Barttfeld et al. 2015; McCormick et al. 2020; Pais-Roldan et al. 2020). The brain dynamic stages can be assessed using eye-tracking (e.g. pupillometry) as an external readout in combination with direct brain functional measurements such as electrophysiological recordings or functional magnetic resonance imaging (fMRI) (McGinley et al. 2015; Chang et al. 2016; Yuzgec et al. 2018; Pais-Roldan et al. 2020). For instance, the slow cortical oscillations of the electrophysiological signals are negatively synchronized with pupil size fluctuations during low arousal states in unconscious animals (Yuzgec et al. 2018). Besides measuring cortical brain state changes, studies in subcortical areas have revealed the involvement of the lateral hypothalamus (LH) and multiple brainstem nuclei including the locus coeruleus (LC) and periaqueductal gray in the regulation of brain states (Saper et al. 2001; Carter et al. 2010; Weber et al. 2015; Liu et al. 2017; Szabadi 2018). In particular, LC-based noradrenergic regulation of the anterior cingulate cortex (ACC) activity is in tight relationship with the pupil size regulation (Carter et al. 2010; Costa and Rudebeck 2016; Reimer et al. 2016; Liu et al. 2017), presenting a crucial link between the ACC activity and different sleep states and wakefulness (Gompf et al. 2010; Rudebeck et al. 2014). It should be noted that the spontaneous change of pupil size and associated brain dynamic stages are not solely dependent on the noradrenergic pathways; instead, they are likely orchestrated by multiple subcortical structures (Costa and Rudebeck 2016; Joshi et al. 2016; DiNuzzo et al. 2019). Interestingly, neural spike rates recorded in the ACC present both positive and negative correlations with pupil size change across trials (Joshi et al. 2016), suggesting more complex subcortical regulation of brain state-dependent pupil dynamics.

The LH is an important hub for brain state regulation (Saper et al. 2001) where different neural cell types co-exist, showing varied activities depending on the underlying arousal state (Adamantidis et al. 2007; Kelz et al. 2008; Hassani et al. 2009; Konadhode et al. 2013). Also, electrical activation of the LH directly causes pupil dilation (Ranson and Magoun 1933). The LH activity has been reported to modulate LC-mediated arousal state and pupil dynamics (Hagan et al. 1999; de Lecea 2015; Herrera et al. 2016). There is anatomical evidence showing direct neural projections of arousal-related nuclei from the LH to the ACC (Jin et al. 2016). However, the functional interaction between the LH and ACC has not been fully investigated to elucidate their impact on brain dynamic stages and pupil dynamics.

Here, we measured brain dynamic stages with pupillometry, electrophysiology in the LH and ACC, and whole-brain fMRI with simultaneous fiber photometry Ca^{2+} recording in the ACC. We first identified a biphasic distribution of the correlation between pupil size and power of local field potential (LFP) in both LH

Received: January 30, 2023. **Revised:** August 7, 2023. **Accepted:** August 8, 2023

and ACC across different trials of recordings. Based on opposite signs of the correlation (positive vs. negative), we discovered two distinct brain dynamic stages and performed cross-frequency coupling analyses to identify brain state-specific characteristics of LFP signals for the two stages. Specifically, the LFP delta (1–4 Hz) phase coupled stronger to amplitudes of higher frequency bands at the ACC in trials where LH-LFP and pupil were negatively correlated, suggesting the trials with negative signs as a lower arousal state (Mukamel et al. 2011; Nair et al. 2016; Pal et al. 2017). Meanwhile, similar to the LFP-based pupil dynamic correlation, the ACC neuronal Ca^{2+} also showed an opposite correlation with pupil dynamics across different trials. Interestingly, in trials with the positive correlation between LH fMRI and pupil dynamics, the ACC Ca^{2+} signal showed a primarily negative correlation with pupil dynamics. This observation suggested that similar brain dynamic stages could be identified in electrophysiology and fMRI measurements based on LH activity. This work revealed unique LH activity patterns with both LFP and fMRI according to its different coupling features with pupil dynamics, which were associated with different brain dynamic stages.

Materials and methods

Subjects

All experiments were performed in accordance with the European Communities Council Directive (2010/63EU) and the German Animal Protection Law and approved by the Animal Protection Committee of Tübingen (Regierungspräsidium Tübingen, Germany). Nine Sprague Dawley rats [Strain: Crl:CD (SD), Sex: Male, Age: 3–6 months, Charles River Laboratories, Sulzfeld, Germany] were used for the multimodal electrophysiology experiments and nine Sprague Dawley rats for the multimodal fMRI experiments. All experiments were performed under alpha-chloralose anesthesia. The multimodal fMRI data had been previously published (Pais-Roldan et al. 2020). Since our study was exploratory research, the sample size was determined based on similar experiments in previous studies (Hutchison et al. 2010; Paasonen et al. 2018).

Surgical procedures for electrophysiology

Prior to the acquisition of the electrophysiology data, rats were anesthetized with 5% isoflurane and orally intubated with a 14-gage cannula. They were ventilated with a mixture of 2% isoflurane, 30% oxygen, and 70% air at 60 ± 1 breaths per minute by a ventilator (CW-SAR-830/AP) during surgery. The body temperature was maintained at 37–38°C by a heating pad. In order to monitor blood pressure and infuse anesthesia intravenously, cannulation of the femoral artery and vein were performed using polyethylene tubes (PE-50). Afterwards, rats were placed pronely on a stereotactic device, and two craniotomies were performed using a drill over the ACC and LH. A tungsten electrode (the resistance at 1 MΩ; FHC Inc) was placed at the ACC (M/L = +0.5 mm, A/P = +1.2 mm, D/V = −1.8 mm) and LH (M/L = +1.5 mm, A/P = −3.2 mm, D/V = −7.8 mm) respectively. A bolus of ∼80 mg/kg alpha-chloralose anesthesia was intravenously administrated into the femoral vein and inhalation of isoflurane was stopped. Afterwards, a mixture of alpha-chloralose (∼25 mg/kg/h) and pancuronium (∼2 mg/kg/h), a paralyzer agent, was continuously infused through an infusion pump during the whole experiment. During the recording, eye drops were not used to ensure a reliable detection of the pupil since the use of eye drops could have interfered with physiological responses of the pupil as well as quality of video images. Once the experiment was done, the location of the electrodes was confirmed by MR imaging (Supplementary Fig. 13).

Data acquisition of electrophysiology signals

The tungsten electrodes positioned in the ACC and LH respectively were connected to our custom-made pre-amplifier (25× gain and 0.1 Hz high pass), and the acquired analog signals were amplified and filtered by MCP-Plus 8 (20× gain and 10 kHz low pass; Alpha Omega LTD). The total amplification was therefore 500. A sliver wire was placed between the skull and skin above the cerebellar region as a reference. The analog signals were converted to digital signals by the CED Power1401-3A (Cambridge Electronic Design), and the digital signals were recorded by Spike2 (CED) software at 25 kHz of sampling rate. To ensure synchronization between electrophysiology and pupil size recordings, the start time to record electrophysiology signals was set to be consistent with the start time of pupil size detection by a MacroRecoder software.

Data acquisition of pupillometry and extraction of pupil diameter

The pupil size was recorded by a customized video camera (dimensions: 30 mm × 21 mm × 15 mm, focal length of the lens: 10 mm; RS-OV7949–1818, Conrad) in a dark room during the experiments. Infrared LED light (880 nm of wavelength) was added in order to acquire a high contrast of the pupil image. The videos were recorded with 30 frames/s, 8 bits per pixel in RGB24, and 628×586 pixels during the electrophysiology experiments and 29.97 frames/s, 8 bits per pixel in RGB24, and 240×352 pixels during the fMRI experiments. The acquired video was processed by the DeepLabCut toolbox (Mathis et al. 2018; Nath et al. 2019) in order to extract the pupil diameter from each video frame. Four points were labeled at the edge of pupil, and the pupil diameter was calculated based on these four points with the following formula.

$$d = \frac{\sqrt{(x_2 - x_1)^2 + (y_2 - y_1)^2} + \sqrt{(x_4 - x_3)^2 + (y_4 - y_3)^2}}{2}$$

The extracted pupil diameter was first smoothed with a 10 point moving average and then down-sampled to 1 point per 1 s window for fMRI synchronization.

Data acquisition of MR scans

Prior to the acquisition of MR scans, the same preparatory surgical procedures for electrophysiology such as femoral cannulation were performed. Anesthesia was also provided as described above. All MR scans were performed on a 14.1 T/26 cm magnet (Magnex, Oxford) with an Avance III console (Bruker, Ettlingen), as previously described (Pais-Roldan et al. 2020). A custom-made elliptic trans-receiver surface coil (∼2 × 2.7 cm) was used for signal transmission and reception. For the acquisition of functional data, a 3D gradient echo echo-planar imaging (GE-EPI) sequence covering the whole brain was used with the following sequence parameters: 1 s repetition time (TR), 12.5 ms echo time (TE), 14° flip angle, $48 \times 48 \times 32$ matrix size, and $400 \times 400 \times 600$ μm resolution. The total scan time was 15 min 25 s (925 TRs) for each EPI sequence. For the registration of MR images to a template, an anatomical RARE image was acquired with the following parameters: 4 s TR, 9 ms TE, 128×128 matrix size, 32 slices, 150 μm in-plane resolution, 600 μm slice thickness, 8× RARE factor.

Data acquisition of Ca^{2+} signals

The GCaMP (AAV5.Syn.GCaMP6f.WPRE.SV40) fluorescence signal was acquired from the ACC (M/L = +0.5 mm, A/P = +1.2 mm, D/V = −1.8 mm) via an optical fiber (FT200-EMT; NA = 0.39; 200 μm diameter, Thorlabs), connected to a light path setup, as previously described (Pais-Roldan et al. 2020). The signals were recorded at 5 kHz sampling rate using an analog input to digital converter in Biopac 150 system (Biopac, Goleta, CA, USA).

Analysis of electrophysiology signals

The acquired data were processed in Matlab. In order to extract the power of LFP signals from every second, spectral analysis using wavelet decomposition was performed with 2 s sliding windows between 0.5 Hz and 100 Hz. The extracted LFP powers were categorized into different frequency bands based on a previous animal sleep study (Yuzgec et al. 2018) as follows: delta (1–4 Hz), theta (4–7 Hz), alpha (7–14 Hz), beta (15–30 Hz), low gamma (30–60 Hz), and high gamma (60–100 Hz). The extracted power time series was first smoothed with a 11 point moving average. The correlation between the power of each frequency band and pupil diameter changes was assessed after synchronizing both signals, using the Matlab corrcoef function.

Coherence

Coherence analysis is a standard method to evaluate functional connection of different brain regions in the frequency domain in electrophysiology studies (Nunez et al. 1997). Prior to evaluating the coherence, the raw data was downsampled from 25,000 to 500 sampling points per second. In the coherence analysis between the ACC and LH electrophysiology recordings sites, the Matlab mscohere function was used to calculate the magnitude-squared coherence with a 2 s Hanning window and an overlap of 1 s. This function has been used to compute functional connectivity measures in electrophysiology studies (Chapeton et al. 2019).

Phase locking value analysis

The phase locking value (PLV) measures synchronization of the phase between two different brain regions to investigate functional connectivity (Lachaux et al. 1999). Prior to calculating the PLV, the raw data was downsampled from 25,000 to 5,000 sampling points per second. The phase of each LFP was extracted using the Morlet wavelet and the fast Fourier transform from LH and ACC LFP signals, respectively. Then, the PLV was calculated with the following formula:

$$PLV = \left| \frac{\sum_{t=1}^{n} e^{i(\phi_{LH(t)} - \phi_{ACC(t)})}}{n} \right|$$

where n represents the number of sampling points, ϕ represents phase angles with the same length of sampling points, and e^i represents the exponential integral.

Phase-amplitude coupling

The phase amplitude coupling, using the modulation index (MI), is a well-used method to evaluate modulation of brain functions; it estimates how the phase of the low-frequency oscillation (e.g. delta band) couples with the amplitude of the high frequency oscillation (e.g. gamma band) (Tort et al. 2010; Mukamel et al. 2011). Prior to calculating the MI, the amplitude of the upper envelope of the LFP signal in each frequency band was extracted using the Matlab envelope function, and the phase angles of each frequency band were extracted using the Matlab hilbert and angle functions. Then, the MI was calculated using the Kullback–Leibler (KL) distance between the amplitude and phase distributions as described in Tort et al. (2010) (Tort et al. 2010) using the "modulation_index" Matlab function (https://github.com/pierremegevand/modulation_index).

Analysis of fMRI signals

The EPI data from each animal were registered to an anatomical scan (RARE) of the corresponding animal. To spatially match data across animals, one RARE scan was used as a template and other anatomical scans were registered to it, while saving the transformation matrices. Finally, the saved transformation matrices were used to register all functional data together. A bandpass filter was applied to the fMRI signals between 0.01 and 0.1 Hz. These fMRI signals were correlated with pupil diameter changes and the power of 1–4 Hz Ca^{2+} signals using the Matlab corr function. With the purpose of comparing the whole brain fMRI map with previous publications (Schneider et al. 2016; Pais-Roldan et al. 2020), the voxel-wise correlation *t*-value was calculated based on the following formula:

$$t = \frac{r\sqrt{n-2}}{\sqrt{1-r^2}}$$

where r represents the correlation coefficient and n represents the number of sampling points from each run. Once the whole brain *t*-value map was generated, it was registered on the anatomical image using the AFNI software package (Cox 1996). In addition, these anatomical scans were overlapped with a rat brain atlas (Paxinos and Watson 2007) to identify the location of brain regions.

Analysis of Ca^{2+} signals

The acquired optical fiber Ca^{2+} signals (GCaMP) were processed by Matlab. The Ca^{2+} signal was first synchronized with fMRI signals with a customized Matlab code. In order to extract the power of Ca^{2+} signals, spectral analysis using wavelet decomposition was performed with 2 s sliding windows between 0.5 Hz and 100 Hz every second. Then, 1–4 Hz of Ca^{2+} powers, equivalent to the delta band of LFP, were extracted. The power of 1–4 Hz Ca^{2+} signals was correlated with pupil diameter changes and fMRI signals using the Matlab corrcoef function.

Analysis to determine the thresholds for the positive, no, and negative correlation

ACC and LH electrophysiology versus pupil

The thresholds for positive and negative correlations were statistically determined by taking the 95% confidence interval from correlations between randomized pupil signals and LFP delta power with 10,000 times of permutation using the Matlab randperm and corrcoef functions (Supplementary Fig. 3). Trials above the upper confidence limit (correlation coefficients >0.065) were defined as positive correlations and those below the lower confidence limit (correlation coefficients < −0.065) as negative correlations. Trials remaining within this 95% confidence interval were considered as uncorrelated. Using the randomized pupil signal, distribution of correlation coefficients with LFP delta power across all trials was examined to assess whether this distribution of correlations with randomized data deviates from the true data. The result shows that distributions between the true and randomized results differ (Fig. 1e, Supplementary Fig. 3), indicating that correlation between pupil and LFP signals are not random.

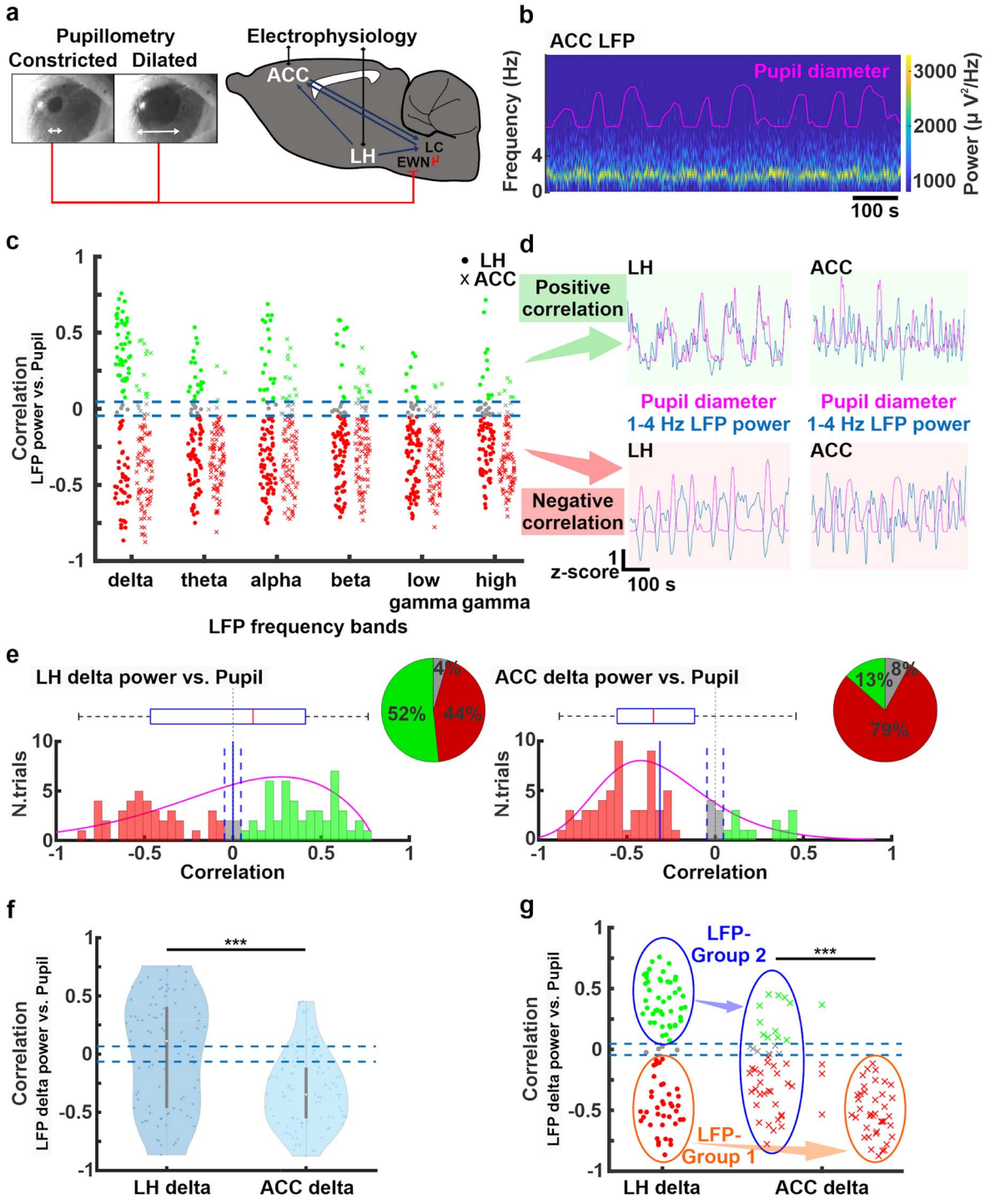

Fig. 1. a) The experimental setup for simultaneous electrophysiology and pupil size recordings. Images of pupillary response (constricted and dilated pupil) are shown. b) Power spectrum of LFP signals in the ACC with pupil diameter fluctuations (pink trace) in a representative rat during 15 min of resting state recording. c) Correlation coefficients between pupil dynamics and power of all LFP bands in the ACC (circular markers) and in the LH (cross markers) from all trials ($n = 89$, 9 animals). Each marker represents the positive (green), no (gray), or negative (red) correlation on each trial. Thresholds of positive (0.046) or negative (−0.046) correlations are shown as blue dashed lines. d) Examples of positive (green shade) and negative (red shade) correlation between pupil dynamics (pink trace) and LFP delta (1–4 Hz) band power fluctuations (blue trace) in the LH and ACC during 15 min of resting state (all plots have the same scale). e) Distribution of correlation coefficients between LFP delta power fluctuation and pupil dynamics in the LH (left; [+ (green)]: $N = 46$, 52%, [0 (gray)]: $N = 4$, 4%, [− (red)]: $N = 39$, 44%) and ACC (right; [+ (green)]: $N = 12$, 13%, [0 (gray)]: $N = 7$, 8%, [− (red)]: $N = 70$, 79%). Each pie chart represents ratios of the positive, no, and negative correlations. Vertical blue solid lines represent the mean of correlation coefficients across all trials in the LH and ACC, respectively. Pink curves and boxplots represent the distribution of trials for LH and ACC, respectively. The vertical black dashed line represents zero. f) Violin plots for the distribution of correlation coefficients between pupil dynamics and LFP delta power fluctuation in LH and ACC. g) Categorization of correlation coefficients in the ACC between LFP delta power fluctuation and pupil dynamics when LH delta power fluctuation has a negative (LFP-group 1, orange) or positive (LFP-group 2, blue) correlation with pupil dynamics. In LFP-group 1, ACC delta power fluctuation and pupil size fluctuation show a negative correlation (correlation coefficient < −0.046) in all trials. In LFP-group 2, correlations of ACC delta power fluctuation and pupil dynamics diversify to a great extent. *Note*: [+]: Correlation coefficient > 0.046, [0]: −0.046 < correlation coefficient < 0.046, [−]: Correlation coefficient < −0.046; ***$P < 0.001$, **$P < 0.01$, *$P < 0.05$.

Pupil versus ACC Ca^{2+}

The thresholds for positive and negative correlations were statistically determined by taking the 95% confidence interval from correlations between randomized pupil signals and 1–4 Hz Ca^{2+} power with 10,000 times of permutation using the Matlab randperm and corrcoef functions (Supplementary Fig. 9). Trials above the upper confidence limit (0.065) were defined as positive correlations and below the lower confidence limit (−0.065) were defined as negative correlations. Otherwise, trials within this 95% confidence interval were considered as no correlation. Using the randomized pupil signal, distribution of correlation coefficients with 1–4 Hz Ca^{2+} power across all trials was examined to see if this distribution of correlations with randomized data deviates from the true data. The result shows that distributions between the true and randomized results differ (Fig. 3d, Supplementary Fig. 9), indicating that correlation between pupil and Ca^{2+} signals are not random.

fMRI versus pupil

The two different brain dynamic stages (positive or no correlation between BOLD fMRI and pupil dynamics) were statistically determined by taking the 95% confidence interval from correlations between the randomized pupil signal and fMRI signal in the LH with 10,000 times of permutation using the Matlab randperm and corr functions. The result shows that the distribution of correlations with randomized data differs from the true data (Supplementary Fig. 12), indicating that correlations between pupil and fMRI signals are not random. Trials above the upper confidence limit (1.96) were defined as positive correlations and those between the upper and lower confidence limit ($-1.96 < CI < 1.96$) were defined as no correlation. The LH region of interest was located in a single slice centered at the same position as electrophysiology LH recordings (33 manually selected voxels at $A/P = -3.2$ mm). *T*-values for correlation were calculated for the whole brain analysis as described above. In addition, the correlation between pupil and each fMRI voxel was corrected by the false discovery rate using the "FDR" Matlab function with alpha 0.05 for 20,022 voxels (https://www.mathworks.com/matlabcentral/fileexchange/71734-fdr-false-discovery-rate). Thereby, the whole-brain maps show voxels of positive correlation with *t*-value >2.54 and negative correlation with *t*-value < −2.54 (Fig. 4c, Supplementary Fig. 11).

fMRI versus ACC Ca^{2+}

T-values for correlation were calculated between the power of 1–4 Hz ACC Ca^{2+} and each fMRI voxel as described above. In addition, the correlation was corrected by the false discovery rate using the "FDR" Matlab function with alpha 0.05 for 20,022 voxels as described above. Thereby, the whole-brain maps show voxels of positive correlation with *t*-value > 2.25 and negative correlation with *t*-value < −2.25 (Fig. 3f and Fig. 4f, Supplementary Fig. 10a and b).

Results

Simultaneous pupillometry and electrophysiology recordings in the ACC and LH

A cycle of brain dynamic stages in anesthetized rats appears with a 10–13 min period on average (Clement et al. 2008; Whitten et al. 2009; Pagliardini et al. 2012), also comparable to the cyclic period of different brain dynamic stages in sleeping rats (Borbély 1976; Trachsel et al. 1991). In this study, LFP was recorded at ACC and LH simultaneously with pupillometry for an epoch duration of 15 min to study the brain state-dependent pupil dynamics in anesthetized rats (Fig. 1a). The LFP power spectrum fluctuation was well-aligned with concurrent pupil diameter changes in a representative trial (Fig. 1b). The correlation between pupil diameter and LFP power in various frequency bands in the LH and ACC varied across trials from negative to positive as well as no coupling, as shown in (89 trials from 9 animals, Fig. 1c and d, Supplementary Fig. 1). The varied correlation patterns were also detected within the same animal (Supplementary Fig. 2). In particular, among all frequencies, the oscillation of the delta (1–4 Hz) power was most prominent throughout the entire recording period (Fig. 1b). Therefore, correlations of delta power with pupil dynamics were further explored to investigate the LFP coupling between LH and ACC.

The correlation between pupil dynamics and LFP delta power fluctuation was more evenly distributed in the LH (positive correlation: 52%, $n = 46$; no correlation: 4%, $n = 4$; negative correlation: 44%, $n = 39$; Fig. 1e left) than the ACC, which showed primarily negative correlation to pupil dynamics (positive correlation: 13%, $n = 12$; no correlation: 8%, $n = 7$; negative correlation: 79%, $n = 70$, Fig. 1e right). The correlation-based distribution patterns between the LH and ACC differed significantly, as assessed using the two-sample Kolmogorov–Smirnov test (Marsaglia et al. 2003) ($P = 5.1 \times 10^{-7}$; Fig. 1f). Based on the positive versus negative correlation features, we specified two groups, which were statistically determined by calculating the 95% confidence interval from 10,000 correlation measures computed between randomized pupil size and LFP delta power signals (Supplementary Fig. 3). When the LH delta power and pupil dynamics were negatively correlated (LFP-Group 1), ACC delta power fluctuation and pupil dynamics were negatively correlated in 100% of cases (Fig. 1g). However, when LH delta power fluctuation and pupil dynamics were positively correlated, possibly indicating a different brain dynamic stage (LFP-Group 2), the correlation patterns between ACC delta power and pupil dynamics exhibited both positive and negative correlation (Fig. 1g). Two-sample *t*-tests showed that correlations of ACC delta power and pupil dynamics between LFP-Group 1 and 2 occurred differently. ($P = 5.2 \times 10^{-10}$; Fig. 1g), possibly suggesting differences in brain dynamic stages based on the relationship between LH and pupil dynamics.

Characterizing distinct brain dynamic stages through cross-frequency coupling analyses

To further investigate two brain dynamic stages identified by distinct coupling features between the LH delta power fluctuation and pupil dynamics (Fig. 1g), we performed cross-frequency coupling analyses. In LFP-Group 1, the LH and ACC exhibited the peak power at 2–2.5 Hz (Fig. 2a, Supplementary Fig. 4). In contrast, in LFP-Group 2 (when the LH delta power fluctuation was positively correlated with pupil dynamics), the LH and ACC exhibited the peak power at 3 Hz (Fig. 2a, Supplementary Fig. 4). Similarly, analyses of both coherence and phase-locking values between the LH and ACC showed the highest values at 2 Hz in LFP-Group 1 but at 3 Hz in LFP-Group 2 (Fig. 2b–d, Supplementary Fig. 5, Supplementary Table 1). Two-sample *t*-tests between LFP-Group 1 and 2 phase-locking values showed significant difference at 2 Hz ($P = 4.8 \times 10^{-7}$) and 3 Hz ($P = 8.8 \times 10^{-7}$). These results indicate that the neuronal coupling between LH and ACC altered between two different states. Moreover, the modulation index, a measurement of the phase-amplitude coupling, between the phase of delta band and amplitudes of all other LFP frequency

bands at the ACC was higher in LFP-Group 1 than LFP-Group 2 (Fig. 2e, Supplementary Table 2). Similar observation was also confirmed at the LH that the modulation index in LFP-Group 1 was higher than LFP-Group 2 except low gamma band (Supplementary Fig. 6, Supplementary Table 3). Two-sample *t*-tests between LFP-Group 1 and 2 showed significant difference on theta band ($P = 1.9 \times 10^{-12}$ for ACC, $P = 2.6 \times 10^{-8}$ for LH), alpha band ($P = 4.6 \times 10^{-12}$ for ACC, $P = 2.4 \times 10^{-7}$ for LH), beta band ($P = 1.9 \times 10^{-11}$ for ACC, $P = 3.2 \times 10^{-8}$ for LH), low gamma band ($P = 1.5 \times 10^{-5}$ for ACC), and high gamma band ($P = 5.9 \times 10^{-8}$ for ACC, $P = 0.0013$ for LH) except low gamma band at the LH ($P = 0.97$). In addition, the results for the separation of two different groups and cross-frequency coupling analyses were consistent with those obtained when a higher threshold (correlation coefficients = 0.15) was used (Supplementary Figs. 7 and 8), suggesting that the use of +/−0.065 correlation coefficients provided physiologically meaningful results. These results validate the presence of two distinct brain dynamic stages involving both LH and ACC under anesthesia, which resembled previous sleep studies (Benoit et al. 2000; Nair et al. 2016; Olbrich et al. 2017) (see Discussion).

Verifying coupling features of neuronal Ca^{2+} signals with simultaneous pupil dynamics and fMRI

To assess the relationship between brain state-dependent pupil dynamics and whole-brain activity, blood oxygen level dependent (BOLD) fMRI with simultaneous pupillometry was performed as previously reported (61 trials from 10 animals) (Pais-Roldan et al. 2020). Meanwhile, we performed fiber photometry to record the GCaMP6-mediated neuronal Ca^{2+} signals in the ACC of these animals, as an alternative to LFP recordings, with better MRI compatibility (Fig. 3a) (Pais-Roldan et al. 2020). Similar to LFP results, the power of ACC Ca^{2+} signals also co-varied with spontaneous pupil size fluctuations (Fig. 3b). The power of 1–4 Hz Ca^{2+} signal in the ACC was primarily negatively correlated with pupil dynamics (positive correlation: 11%, $n = 7$; no correlation: 20%, $n = 12$; negative correlation: 69%, $n = 42$; Fig. 3c and d), which was consistent with our electrophysiology results (Fig. 1e). The clustering of varied correlation features between the 1–4 Hz Ca^{2+} power fluctuation and pupil dynamics among different trials was determined based on the 95% confidence interval calculated by permutation (Supplementary Fig. 9). Besides pupil dynamics, ACC neuronal Ca^{2+} signal also showed positive and negative correlation with fMRI signals across different brain regions and trials (Fig. 3e, Supplementary Fig. 10a). Interestingly, in trials with a negative correlation between 1 and 4 Hz Ca^{2+} power fluctuation and pupil dynamics, the Ca^{2+} power fluctuation showed a positive correlation with fMRI fluctuation in cortical and thalamic areas but a negative correlation in subcortical areas, including the LH (Fig. 3e and f). In other trials, no significant correlation was detected between fMRI and the ACC Ca^{2+} power fluctuation (Supplementary Fig. 10b). These multimodal fMRI results indicated that correlation features between Ca^{2+}-based neuronal fluctuation of the ACC and BOLD fMRI signals vary among different brain regions according to different anesthetized brain dynamic stages.

Classifying distinct brain dynamic stages based on LH BOLD fMRI and pupil dynamics

Next, we examined if LH BOLD signal could be used to differentiate brain state-dependent pupil dynamics across different trials, as evaluated with LFP data in previous experiments. First, we created a mean correlation map between fMRI and pupil dynamics, showing a global negative correlation pattern as previously reported (Supplementary Fig. 11) (Pais-Roldan et al. 2020). Moreover, similar to the fMRI-Ca^{2+} correlation, the trial-specific correlation patterns between pupil dynamics and fMRI showed varied signs across different brain regions (Fig. 4a, Supplementary Fig. 11). In particular, at the LH, the *t*-value of correlation coefficient varied extensively across individual trials, showing positive (33%, $n = 20$) or no (67%, $n = 41$) correlations (Fig. 4b). We statistically determined this positive correlation by calculating the 95% confidence interval from 10,000 repetitions of correlation measures between randomized pupil signals and each LH fMRI voxel (Supplementary Fig. 12). In trials showing positive signs, robust positive correlation was also observed between the pupil dynamics and fMRI signal in the brainstem and basal forebrain regions but negative correlation was detected in thalamic and cortical regions (Fig. 4c), which was not detected in trials with no correlation between LH fMRI and pupil dynamics (Fig. 4c). Notably, when exploring the correlation of pupil dynamics and ACC 1–4 Hz Ca^{2+} power from the trials with the positive LH fMRI-pupil correlation sign, all of the ACC Ca^{2+}-pupil correlation coefficients were negative (Fig. 4d and e; fMRI-Group 1). This observation was consistent with the electrophysiological results when differentiating LFP-Group 1 and 2 based on LH LFP-pupil relationship (Fig. 1f). Two-sample *t*-tests for correlations of ACC 1–4 Hz Ca^{2+} power with pupil dynamics between fMRI-Group 1 and 2 showed a significant difference ($P = 3.7 \times 10^{-4}$; Fig. 4d). It should be noted that in LFP-Group 1 the negative LH LFP (delta power)-pupil correlation predicted the negative correlation of ACC LFP (delta power)-pupil correlation, while in the fMRI-Group 1 it was the positive LH-pupil correlation which predicted the negative ACC Ca^{2+}-pupil correlation. This might be due to an anti-correlation between BOLD fMRI and delta power in the LH (Jaime et al. 2019) (see Discussion). In addition, whole-brain fMRI BOLD and ACC Ca^{2+} power coupling was higher in fMRI-Group 1 than fMRI-Group 2 (Fig. 4f), indicating distinct brain dynamic stages associated to the different groups. Overall, these results indicate that correlation of LH fMRI-pupil dynamics can identify distinct brain dynamic stages, similar to the LH-ACC observations of LFP-based brain dynamic stages.

Discussion

In the present study, we reported distinct coupling features between brain activity and pupillometry in anesthetized rats, presenting either positive or negative correlation based on multimodality measurements. When the LH LFP delta power fluctuation was negatively correlated to pupil size changes, the ACC LFP-pupil correlation was always negative. In contrast, varied correlation features of ACC-pupil were detected when the LH was positively correlated to pupil dynamics. Based on the LH-pupil relationship, we identified distinct cross-frequency coupling features of the LFP signals detected in the LH and ACC, defining two different anesthetized brain dynamic stages (LFP-Group 1 vs. 2). In parallel, the trial-specific ACC Ca^{2+}-pupil correlation was associated with the fMRI-based LH-pupil relationship similar to the LFP results. In summary, two distinct brain dynamic stages could be identified based on the LH-pupil relationship, which could be verified by analyzing the site-specific LFP cross-frequency coupling or whole-brain fMRI-based Ca^{2+} and pupil correlation patterns.

The brain state embraces a broad number of distinctive features physiologically and behaviorally that can be observed across multiple scales (Kringelbach and Deco 2020; McCormick et al. 2020). These can be as evident as those differentiating sleep

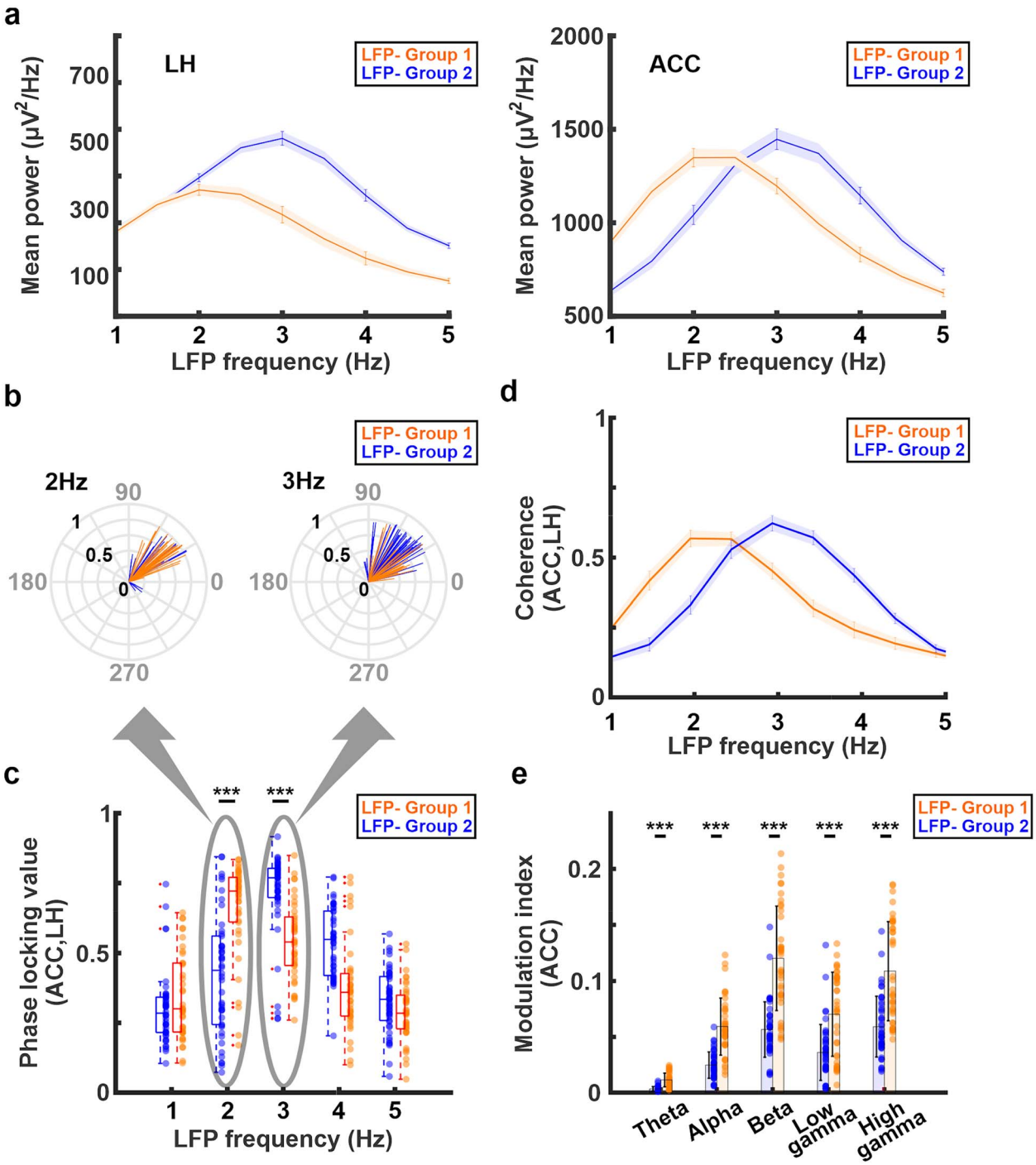

Fig. 2. a) Power spectrum density of the LH (left) and ACC (right) in LFP-group 2 (blue line) and LFP-group 1 (orange line). The shaded areas represent the standard error of the mean. The peak frequency in both LH and ACC is at 3 Hz in LFP-group 2 (blue line) but at 2 Hz in LFP-group 1 (orange line). b) The radial plots of the trial-specific phase angles ([degrees], gray) and phase-locking value (black) between LH and ACC at 2 Hz and 3 Hz in LFP-group 1 (orange) and LFP-group 2 (blue). c) Phase locking value between the LH and ACC in both groups. The highest phase synchrony occurred at 3 Hz in LFP-group 2 (blue) but at 2 Hz in LFP-group 1 (orange). d) Magnitude squared coherence between LH and ACC. The highest coherence occurred at 3 Hz in LFP-group 2 (blue) but at 2 Hz in LFP-group 1 (orange). The shaded areas represent the standard error of the mean. e) Phase-amplitude coupling using the modulation index (MI) at the ACC between the phase of delta (1–4 Hz) band and amplitude of other frequency bands. The MI in LFP-group 1 (orange) is higher than LFP-group 2 (blue) on all frequency bands. Error bars indicate the standard deviation. *Note*: ***$P < 0.001$, **$P < 0.01$, *$P < 0.05$.

from wakefulness (e.g. readily observed as electrophysiological transitions) (Adamantidis et al. 2007; Yuzgec et al. 2018) or much less apparent, which is the case when assessing varying brain dynamic stages under anesthesia. An example of the latter scenario is provided here in the form of changes that we reliably observed only after multi-modal analysis in our data. In order to detect the features of complex brain states, exploratory analyses complementary to routine electrophysiology assessments are commonly used, such as cross frequency analysis in electrophysiology and correlation analysis between pupil diameters and fMRI/electrophysiology signals (McGinley et al. 2015; Yellin et al. 2015; Yuzgec et al. 2018; Migliorelli et al. 2019).

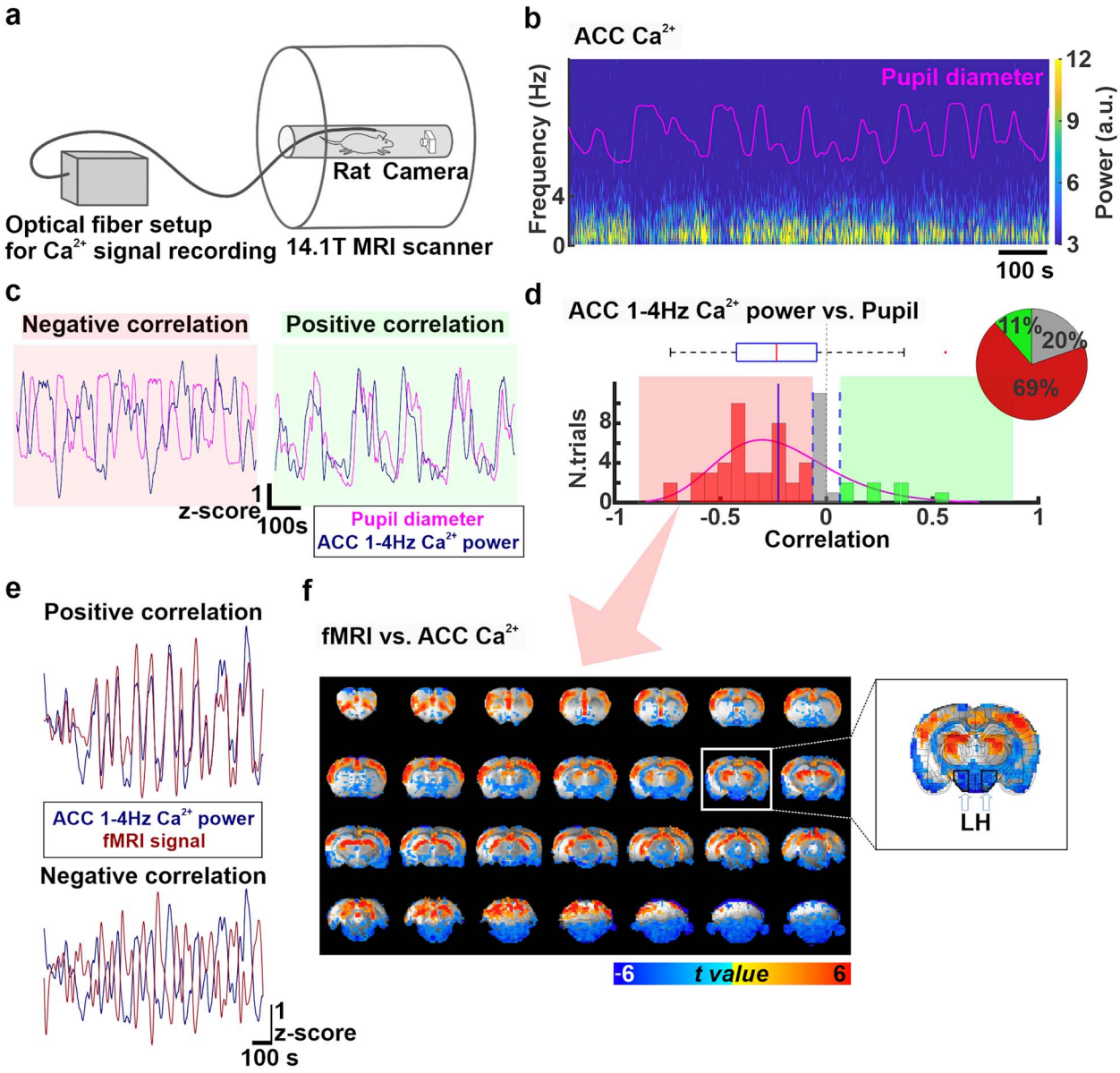

Fig. 3. a) The experimental setup for multimodal resting-state BOLD fMRI recordings simultaneously with measurements of optical fiber Ca^{2+} signals and pupil dynamics. b) Power spectrum of ACC Ca^{2+} signals during 15 min of resting-state along with changes in pupil diameter (pink trace) in a representative rat. A.u: Arbitrary units. c) Examples of positive (right, green) and negative (left, red) correlations between pupil dynamics (pink) and ACC 1–4 Hz Ca^{2+} power fluctuation (navy blue) during 15 min of resting state. d) Distribution of correlation coefficients between pupil dynamics and ACC 1–4 Hz Ca^{2+} power fluctuation for all trials ($n = 61$, 10 animals). These correlation coefficients are negative (correlation coefficient < -0.064) in 69% ($n = 42$, red), none ($-0.064 <$ correlation coefficient < 0.064) in 20% ($n = 12$, gray), and positive (correlation coefficient > 0.064) in 11% ($n = 7$) of the trials. The pie chart represents ratios of the positive, no, and negative correlations. e) Examples of positive and negative correlation between fMRI signal (brown) and ACC 1–4 Hz Ca^{2+} power (navy blue) fluctuations during 15 min of resting state. f) *t*-value maps of correlation between ACC 1–4 Hz Ca^{2+} power and each fMRI voxel when ACC 1-4 Hz Ca^{2+} power fluctuation and pupil dynamics were negatively correlated during 15 min of resting state ($n = 42.69\%$). The overlay shows voxels with *t*-value < -2.25 and *t*-value > 2.25. A coronal slice at coordinates $A/P = -3.2$ mm is shown magnified on the right, where the location of the LH is indicated with white arrows and black polygons.

In this study, we investigated the coupling features between pupil size and LFP power and between pupil size and fMRI signal during 15 min of recording sessions to evaluate different brain dynamic stages in anesthetized animals. Our results showed two opposite correlation patterns between pupil dynamics and LFP measured at the LH and ACC as well as different fMRI-pupil synchronization across trials (Fig. 5), which we interpreted as surrogates of distinct states of the brain. Importantly, our definition of brain state is based on our available multimodal observations (pupil size, two-point electrophysiology, fMRI, and calcium recordings); it should be noted that more complex or even a mixture of several brain states could give rise to the states here-identified.

It is known that the neural activity in the LH plays an important role in changing and maintaining an ongoing brain state during wakefulness, sleep, and anesthesia (Saper et al. 2001; Kelz et al. 2008; Herrera et al. 2016; Yin et al. 2019). Awake-promoting neurons in the LH (e.g. orexin-producing neurons) reduce their neural firing during both slow-wave sleep (Lee et al. 2005) and anesthesia (Kelz et al. 2008). The anesthetized brain mimics different sleep stages (Vacas et al. 2013), suggesting common regulatory

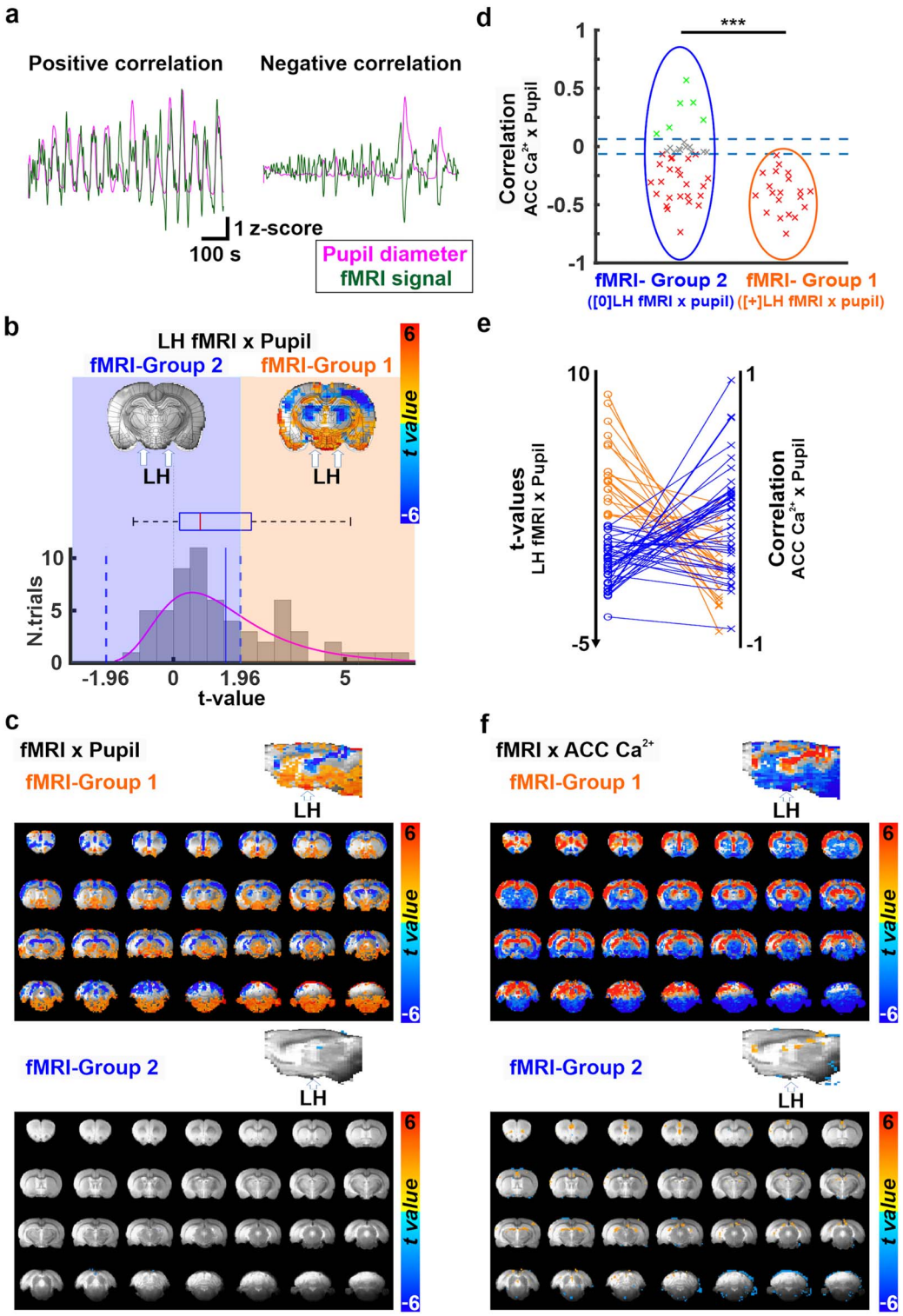

Fig. 4. a) Examples of positive (left) and negative (right) correlations between pupil dynamics (pink) and fMRI signal fluctuations (green) during 15 min of resting state. b) The representation of two distinct brain states. Trials are sorted into two groups characterized by positive (fMRI-group 1) or no (fMRI-group 2) correlation between the LH BOLD fMRI signal and the pupil size fluctuations. On the top, two fMRI-pupil correlation maps at A/P = −3.2 mm from fMRI-group 1 and 2 are shown. The location of LH is indicated with a white arrow. The bottom graph represents the *t*-value distribution of the LH-fMRI and pupil dynamics correlations across all trials ($n = 61$), on which the state differentiation is based. fMRI-group 1 (positive correlation) was observed in 33% of the trials ($n = 20$, $t > 1.96$), and fMRI-group 2 (no-correlation) in 67% of trials ($n = 41$, $t < 1.96$). c) Whole-brain maps and their sagittal plane view of the correlation between fMRI and pupil dynamics from trials associated with fMRI-group 1 (top) and 2 (bottom). d) Correlation coefficients between pupil dynamics and ACC 1–4 Hz Ca^{2+} power fluctuation sorted by fMRI-group 1 (orange ellipse) and 2 (blue ellipse). The thresholds of correlation coefficients are set at +/− 0.064. e) the plot shows the correspondence between two kinds of analysis in the same data: Correlation *t*-values between LH-fMRI and pupil (left) and the correspondent ACC 1–4 Hz Ca^{2+} power and pupil dynamic correlation for each trial (right). The color indicates the groups (orange for fMRI-group 1 and blue for fMRI-group 2) associated with each trial. f) *t*-value whole-brain maps showing the correlation between fMRI and ACC 1–4 Hz Ca^{2+} power from trials assigned to fMRI-group 1 (top) and 2 (bottom). The overlay shows voxels with *t*-value < −2.54 and *t*-value > 2.54. *Note*: $^{***}P < 0.001$, $^{**}P < 0.01$, $^{*}P < 0.05$.

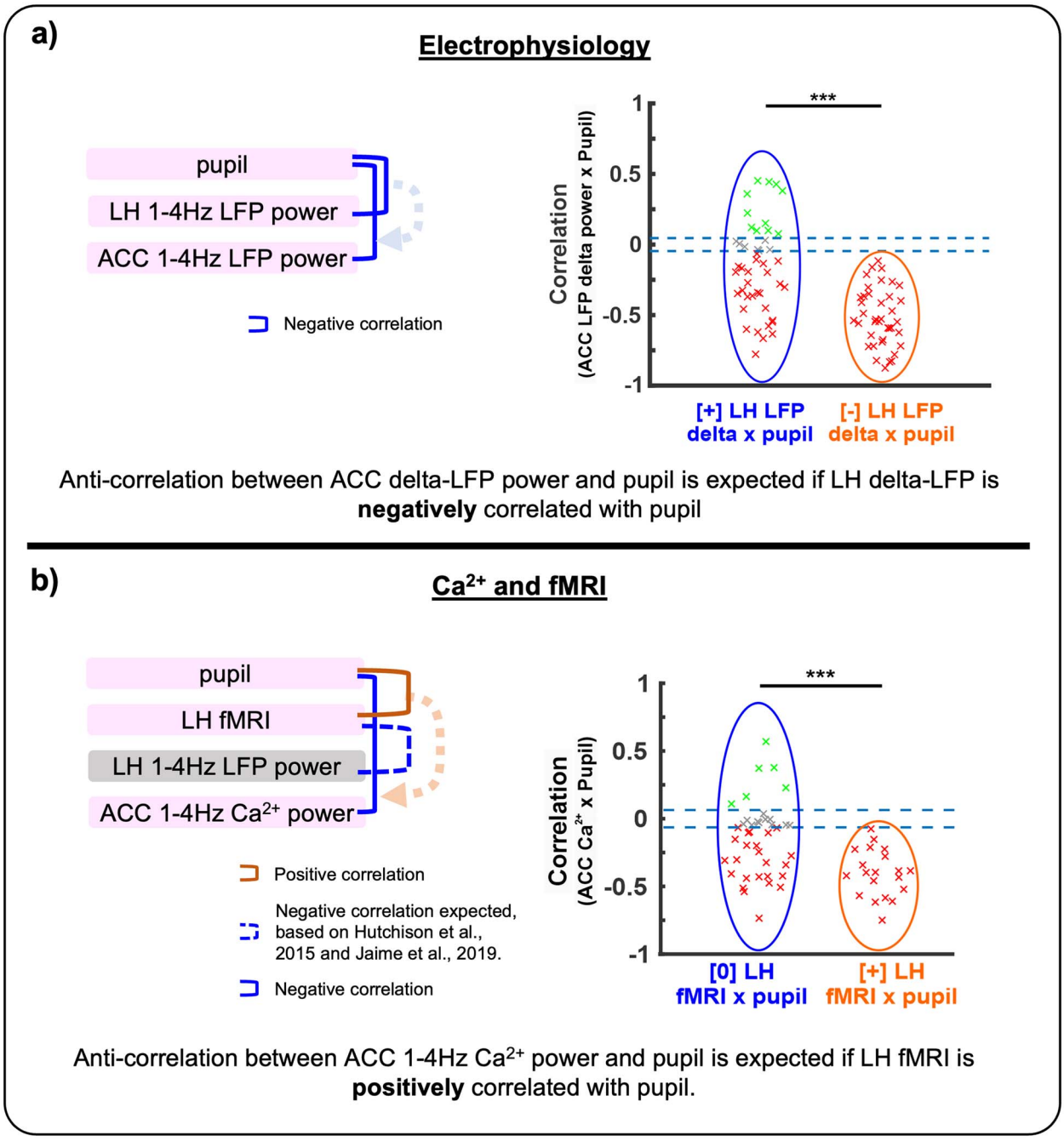

Fig. 5. A schematic diagram showing the sign of correlations across multimodal measurements. a) Correlations between pupil diameter and electrophysiology at the LH and ACC are described. Negative correlations between ACC LFP delta power and pupil diameter were always identified when LH LFP delta power was negatively correlated with pupil diameter. b) Correlations between pupil diameter and 1–4 Hz Ca^{2+} power at the ACC as well as fMRI signals at the LH are described. Negative correlations between ACC 1–4 Hz Ca^{2+} power and pupil diameter were always identified when the LH fMRI signal was positively correlated with pupil diameter. Negative correlation between LH fMRI and LH 1–4 Hz LFP power is also expected from previous works mentioned in the figure.

mechanisms to control the brain dynamic stages. In addition, optogenetic activation of awake promoting neurons in the LH produces cortical arousal and behaviorally awaking from anesthesia (Herrera et al. 2016) or sleep (Adamantidis et al. 2007). Under anesthesia, the neural firing of melanin-concentrating hormone neurons, promoting sleep (Konadhode et al. 2013), are unaffected in spite of the reduced neural firing in awake promoting neurons (Kelz et al. 2008). Therefore, different neural populations in the LH may contribute to the varied coupling features of pupil dynamics at different arousal states even under anesthesia. Moreover, the LH activation causes pupil dilation (Ranson and Magoun 1933) due to inhibition of Edinger Westphal Nucleus (EWN) (Koss et al. 1984; Szabadi 2018). These attributes of the LH support our observation of two opposite correlation patterns (positive and negative) between the neuronal oscillation in the LH and the pupil dynamics (Fig. 1c and d).

We also revealed a unique LH-ACC interaction underlying the varied brain state-dependent pupil dynamics. The ACC is an important hub of the default mode network in both humans and rats (Lu et al. 2012), and its involvement in the resting-state

connectivity has been observed to differ between high and low arousal states, showing a decreased participation of the ACC in the default mode network during the lower arousal state compared to higher state (Horovitz et al. 2009; Tarun et al. 2021). The neural activity in the ACC has been linked to arousal fluctuation and associated with pupil size changes, which can be explained by its bidirectional connection to the noradrenergic LC (Gompf et al. 2010; Ebitz and Platt 2015; Joshi et al. 2016; Pais-Roldan et al. 2020). The opposite correlation features between ACC activity and pupil dynamics (Fig. 1c–e, Supplementary Fig. 2) could not be solely explained by noradrenergic projections from the LC. Given the functional and anatomical interaction between LH and ACC (Saper et al. 2001; Morgane et al. 2005; Gompf et al. 2010; Stevens et al. 2011; Jin et al. 2016), our work suggested that LH can play a pivotal role to mediate subcortical regulation of the ACC activity underlying brain state-dependent pupil dynamics. In the state when the LH delta power fluctuation was negatively correlated with pupil dynamics, the ACC LFP-pupil showed negative correlation (Fig. 1g). This LFP-based Group 1 likely corresponds to a lower arousal level based on evidence from the previous electrocorticogram (ECoG) study with pupil size measurements (Yuzgec et al. 2018); they demonstrated that cortical ECoG-based delta amplitude and pupil dynamics showed very low correlation during wakefulness but strong negative correlation during NREM sleep or moderate negative correlation during REM sleep. We also performed cross-frequency analyses of the LFP signals detected in the ACC and LH, which showed distinct LFP coupling features between LFP-Group 1 and 2 (Fig. 2b). Of note, this spectral-based differentiation of brain dynamic stages is in agreement with sleep EEG studies showing that during NREM sleep, i.e. the deepest state of unconsciousness, the cortical activity peaks ~2 Hz (Benoit et al. 2000; Rodenbeck et al. 2006; Olbrich et al. 2017). In contrast, during REM sleep, i.e. a state of relative awareness, the frequency peak of the EEG shifts to higher values (e.g. 2.5–3 Hz in frontal-central cortical regions) (Olbrich et al. 2017; Bernardi et al. 2019). We also observed the shift of power spectrum between the two LFP groups. The peak of power spectrum in the ACC was at 2 Hz in the trials where we observed negative correlations between the LH activity and pupil size but 3 Hz in the trials where we observed positive correlations (Fig. 2a, right). This shift indicates the changes of spontaneous activity in the ACC. Whether the observed changes in the ACC reflect a direct interaction of the ACC and LH remains unclarified. Future studies using optogenetics or an equivalent technique combined with calcium imaging/electrophysiology could potentially help clarifying the direct influence of one area on another upon the brain dynamic stages. Besides the frequency-specific coupling features of neural firing in the ACC and LH, the magnitude-squared coherence and phase locking analyses also showed distinct values between LFP-Group 1 and 2, which is similar to previous reports of brain state switches from conscious wakefulness to unconsciousness (e.g. anesthetized or deep sleep state) (Ishizawa et al. 2016; Miyamoto et al. 2016; Migliorelli et al. 2019). Since previous studies report that phase-amplitude coupling appears stronger in deeper anesthetized or sleep states (Mukamel et al. 2011; Nair et al. 2016; Pal et al. 2017), our work strongly suggests that the trials in LFP-Group 1 are at a lower arousal level than those in LFP-Group 2.

Pupil dynamics track changes in brain states, in particular, when combined with fMRI as a non-invasive arousal indicator (Yellin et al. 2015; Chang et al. 2016; Schneider et al. 2016). It has been shown that pupil dilation occurs concurrently with global negative BOLD-fMRI signal in anesthetized rats (Pais-Roldan et al. 2020), which coincides with decreased low-frequency power recorded in the cortex in both sleeping and anesthetized animals (Blasiak et al. 2013; Yuzgec et al. 2018). It should be noted that the correlation features between pupil dynamics and fMRI or electrophysiological signals depend on the underlying brain dynamic stages (Yellin et al. 2015; Yuzgec et al. 2018; Pais-Roldan et al. 2020). Based on the fMRI signal detected in the LH, we have defined fMRI-Group 1 for positive correlation with pupil dynamics (33% of trials) and fMRI-Group 2 without significant correlation (~67% of trials) (Fig. 4b). Our results also showed brain-wide cortical negative fMRI correlation with pupil dynamics in fMRI-Group 1 but the negative correlation was not observed in fMRI-Group 2 (Fig. 4c). It is plausible that fMRI-Group 1 corresponds to a lower arousal state than fMRI-Group 2, similar to what has been defined by the LFP-Groups. Indeed, under this positive correlation between LH fMRI and pupil dynamics (fMRI-Group 1), we observed that Ca^{2+}-based neuronal signals in the ACC and pupil dynamics were always negatively correlated, a result that is consistent with our electrophysiology findings (Fig. 4d and Fig. 1g). Furthermore, our BOLD fMRI and Ca^{2+}-based neural correlations were higher in fMRI-Group 1 than in fMRI-Group 2 (Fig. 4f), indicating a change in brain dynamic stages based on LH fMRI-pupil relationships.

A healthy brain during resting-state transits between different states that can be identified based on correlation patterns (Tagliazucchi and Laufs 2014; Barttfeld et al. 2015; Zhou et al. 2019), and their relevance to clinical studies has been demonstrated (Ahmadi et al. 2021; Wu et al. 2021), implying that states identified through correlation changes are biologically meaningful. Although fMRI-pupil interaction shows a promising indicator to estimate brain dynamic stages noninvasively, more efforts remain needed to better elucidate the dynamic coupling features of fMRI and neuronal signals during brain state fluctuation across different brain regions (Mukamel et al. 2005; He et al. 2008; Conner et al. 2011; Magri et al. 2012). In the cortex, He et al. (He et al. 2008) demonstrated varied correlation between electrophysiological and BOLD signals in awake state and slow wave sleep. Furthermore, depending on eye open/closed arousal states in monkeys, correlation features between fMRI and LFP signals vary (Scholvinck et al. 2010), and these eye behaviors can track arousal states with fMRI (Chang et al. 2016). The fiber photometry-based Ca^{2+} (GCaMP) recording with simultaneous fMRI (He et al. 2018) revealed the brain state-dependent correlation features of BOLD signal with neuronal and astrocytic Ca^{2+} signaling, relying on the neuromodulation from thalamic or brainstem nuclei (Wang et al. 2018; Pais-Roldan et al. 2020). In our work, ACC 1–4 Hz Ca^{2+} power fluctuation was positively correlated with BOLD fMRI signals of the entire cortex (Fig. 3f, Supplementary Fig. 10a). In contrast, it was negatively correlated with BOLD fMRI in various subcortical regions including the LH, brainstem, and striatum (Fig. 3f, Supplementary Fig. 10a). Given the positive coupling feature between LH and ACC LFP data as described in LFP-Group 1, the positive correlation of LH fMRI with pupil dynamics in fMRI-Group 1 suggested negative correlation between LH fMRI and LFP. This negative correlation between BOLD fMRI and LFP low-frequency power, in particular at the delta band, has been previously observed in several brain regions including subcortical areas (e.g. striatum) (Hutchison et al. 2015; Jaime et al. 2019), suggesting a non-linear relationship between the neuronal and the vascular network, which is not totally understood.

In this study, we used alpha-chloralose anesthesia to obtain higher quality of BOLD fMRI responses (Hyder et al. 1994; de Celis et al. 2011). The use of alpha-chloralose induces slow-wave activities in the animal's brain (He et al. 2018; Pais-Roldan et al. 2020). Although this anesthetic stably maintains unconsciousness

of animals, the state of brain dynamics fluctuates across time (Wang et al. 2018). In fact, our pupillometry shows that pupil size and LFP signals simultaneously change across time (Fig. 1b). Previous studies showed that different anesthetics (e.g. Urethane and isoflurane) also induced different dynamics of electrophysiological signals and simultaneous pupil size changes (Blasiak et al. 2013; Kum et al. 2016), similar to state-dependent changes of pupil size during different sleep stages (Yuzgec et al. 2018). Moreover, a recent study has also claimed state-dependent correlations between pupil size and both cortical blood volume and LFP, showing negative correlations during a naturally occurring deep unconscious state (NREM sleep) but positive during a shallow unconscious state (REM sleep) (Turner et al., 2023). These observations are comparable with our study that both LFP and BOLD fMRI signals show positive and negative correlations with pupil size depending on different brain dynamic stages. Although the mechanism of how different anesthetics or naturally occurring brain dynamic stages work can differ, our study presents a basis of common systemic features on pupil size and brain dynamics. This above content is now added in the discussion of the manuscript.

In summary, we reported varied brain state-dependent coupling features which are orchestrated in multiple regions (e.g. LH and ACC) and cross multiple scales (frequency and amplitude of neuronal firing, inter-region coherence, brain-wide fMRI, pupillary coupling, etc). This work offers a reference framework to understand the LH-ACC relationship, and, more importantly, it presents a novel way to track brain dynamic stage transitions by bridging pupillary changes with the LH activity. We demonstrate that LH LFP and fMRI signals provide a strong indication of the vigilance level; hence, we anticipate that their assessment may constitute a useful approach to evaluate the ongoing brain states in arousal-related clinical research.

Acknowledgments

We thank Dr R. Pohmann, Dr K. Buckenmaier, Ms H. Schulz, and Dr J. Engelmann for technical support, Dr E. Weiler, Dr P. Douay, and Dr R. König for animal protocol and maintenance support, and Mr M. Arndt and Mr O. Holder for electrical support.

Author contributions

Kengo Takahashi (Conceptualization, Data curation, Formal analysis, Investigation, Methodology, Software, Writing—original draft, Writing—review & editing), Filip Sobczak (Software, Writing—review & editing), Patricia Pais-Roldán (Data curation, Writing—review & editing), and Xin Yu (Conceptualization, Funding acquisition, Methodology, Supervision, Writing—review & editing).

Supplementary material

Supplementary material is available at *Cerebral Cortex* online.

Funding

This research was supported by internal funding from Max Planck Society, NIH Brain Initiative funding (RF1NS113278, 1R01NS122904, R01MH111438), NSF grant (2123971) and shared instrument grant (S10 MH124733-01), German Research Foundation (DFG) YU215/2-1 and Yu215/3-1, BMBF 01GQ1702.

Conflict of interest statement: None declared.

Data availability

The data are available from the corresponding author upon request.

References

Adamantidis AR, Zhang F, Aravanis AM, Deisseroth K, de Lecea L. Neural substrates of awakening probed with optogenetic control of hypocretin neurons. *Nature*. 2007:450(7168):420–424.

Ahmadi M, Kazemi K, Kuc K, Cybulska-Klosowicz A, Helfroush MS, Aarabi A. Resting state dynamic functional connectivity in children with attention deficit/hyperactivity disorder. *J Neural Eng*. 2021:18(4):0460d1.

Barttfeld P, Uhrig L, Sitt JD, Sigman M, Jarraya B, Dehaene S. Signature of consciousness in the dynamics of resting-state brain activity. *Proc Natl Acad Sci USA*. 2015:112(3):887–892.

Benoit O, Daurat A, Prado J. Slow (0.7-2 Hz) and fast (2-4 Hz) delta components are differently correlated to theta, alpha and beta frequency bands during NREM sleep. *Clin Neurophysiol*. 2000:111(12):2103–2106.

Bernardi G, Betta M, Ricciardi E, Pietrini P, Tononi G, Siclari F. Regional Delta waves in human rapid eye movement sleep. *J Neurosci*. 2019:39(14):2686–2697.

Blasiak T, Zawadzki A, Lewandowski MH. Infra-slow oscillation (ISO) of the pupil size of urethane-anaesthetised rats. *PLoS One*. 2013:8(4):e62430.

Borbély AA. Sleep and motor activity of the rat during ultra-short light-dark cycles. *Brain Res*. 1976:114(2):305–317.

Brown EN, Lydic R, Schiff ND. General anesthesia, sleep, and coma. *N Engl J Med*. 2010:363(27):2638–2650.

Carter ME, Yizhar O, Chikahisa S, Nguyen H, Adamantidis A, Nishino S, Deisseroth K, de Lecea L. Tuning arousal with optogenetic modulation of locus coeruleus neurons. *Nat Neurosci*. 2010:13(12):1526–1533.

Chang C, Leopold DA, Scholvinck ML, Mandelkow H, Picchioni D, Liu X, Ye FQ, Turchi JN, Duyn JH. Tracking brain arousal fluctuations with fMRI. *Proc Natl Acad Sci USA*. 2016:113(16):4518–4523.

Chapeton JI, Haque R, Wittig JH, Inati SK, Zaghloul KA. Large-scale communication in the human brain is rhythmically modulated through alpha coherence. *Curr Biol*. 2019:29(17):2801-+–2811.e5.

Clement EA, Richard A, Thwaites M, Ailon J, Peters S, Dickson CT. Cyclic and sleep-like spontaneous alternations of brain state under urethane anaesthesia. *PLoS One*. 2008:3(4):e2004.

Conner CR, Ellmore TM, Pieters TA, DiSano MA, Tandon N. Variability of the relationship between electrophysiology and BOLD-fMRI across cortical regions in humans. *J Neurosci*. 2011:31(36):12855–12865.

Costa VD, Rudebeck PH. More than meets the eye: the relationship between pupil size and locus Coeruleus activity. *Neuron*. 2016:89(1):8–10.

Cox RW. AFNI: software for analysis and visualization of functional magnetic resonance neuroimages. *Comput Biomed Res*. 1996:29(3):162–173.

de Celis AB, Makarova T, Hess A. On the use of α-chloralose for repeated BOLD fMRI measurements in rats. *J Neurosci Methods*. 2011:195(2):236–240.

de Lecea L. Optogenetic control of hypocretin (orexin) neurons and arousal circuits. *Curr Top Behav Neurosci*. 2015:25:367–378.

DiNuzzo M, Mascali D, Moraschi M, Bussu G, Maugeri L, Mangini F, Fratini M, Giove F. Brain networks underlying Eye's pupil dynamics. *Front Neurosci-Switz*. 2019:13:965.

Ebitz RB, Platt ML. Neuronal activity in primate dorsal anterior cingulate cortex signals task conflict and predicts adjustments in pupil-linked arousal. *Neuron*. 2015:85(3):628–640.

Gompf HS, Mathai C, Fuller PM, Wood DA, Pedersen NP, Saper CB, Lu J. Locus ceruleus and anterior cingulate cortex sustain wakefulness in a novel environment. *J Neurosci*. 2010:30(43):14543–14551.

Hagan JJ, Leslie RA, Patel S, Evans ML, Wattam TA, Holmes S, Benham CD, Taylor SG, Routledge C, Hemmati P, et al. Orexin a activates locus coeruleus cell firing and increases arousal in the rat. *Proc Natl Acad Sci USA*. 1999:96(19):10911–10916.

Hassani OK, Lee MG, Jones BE. Melanin-concentrating hormone neurons discharge in a reciprocal manner to orexin neurons across the sleep-wake cycle. *Proc Natl Acad Sci USA*. 2009:106(7):2418–2422.

He BJ, Snyder AZ, Zempel JM, Smyth MD, Raichle ME. Electrophysiological correlates of the brain's intrinsic large-scale functional architecture. *Proc Natl Acad Sci USA*. 2008:105(41):16039–16044.

He Y, Wang M, Chen X, Pohmann R, Polimeni JR, Scheffler K, Rosen BR, Kleinfeld D, Yu X. Ultra-slow single-vessel BOLD and CBV-based fMRI spatiotemporal dynamics and their correlation with neuronal intracellular calcium signals. *Neuron*. 2018:97(4):925–939.e5.

Herrera CG, Cadavieco MC, Jego S, Ponomarenko A, Korotkova T, Adamantidis A. Hypothalamic feedforward inhibition of thalamocortical network controls arousal and consciousness. *Nat Neurosci*. 2016:19(2):290–298.

Horovitz SG, Braun AR, Carr WS, Picchioni D, Balkin TJ, Fukunaga M, Duyn JH. Decoupling of the brain's default mode network during deep sleep. *Proc Natl Acad Sci USA*. 2009:106(27):11376–11381.

Hutchison RM, Mirsattari SM, Jones CK, Gati JS, Leung LS. Functional networks in the anesthetized rat brain revealed by independent component analysis of resting-state FMRI. *J Neurophysiol*. 2010:103(6):3398–3406.

Hutchison RM, Hashemi N, Gati JS, Menon RS, Everling S. Electrophysiological signatures of spontaneous BOLD fluctuations in macaque prefrontal cortex. *NeuroImage*. 2015:113:257–267.

Hyder F, Behar KL, Martin MA, Blamire AM, Shulman RG. Dynamic magnetic resonance imaging of the rat brain during forepaw stimulation. *J Cereb Blood Flow Metab*. 1994:14(4):649–655.

Ishizawa Y, Ahmed OJ, Patel SR, Gale JT, Sierra-Mercado D, Brown EN, Eskandar EN. Dynamics of Propofol-induced loss of consciousness across primate neocortex. *J Neurosci*. 2016:36(29):7718–7726.

Jaime S, Gu H, Sadacca BF, Stein EA, Cavazos JE, Yang Y, Lu H. Delta rhythm orchestrates the neural activity underlying the resting state BOLD signal via phase-amplitude coupling. *Cereb Cortex*. 2019:29(1):119–133.

Jin J, Chen Q, Qiao Q, Yang L, Xiong J, Xia J, Hu Z, Chen F. Orexin neurons in the lateral hypothalamus project to the medial prefrontal cortex with a rostro-caudal gradient. *Neurosci Lett*. 2016:621:9–14.

Joshi S, Li Y, Kalwani RM, Gold JI. Relationships between pupil diameter and neuronal activity in the locus Coeruleus, colliculi, and cingulate cortex. *Neuron*. 2016:89(1):221–234.

Kelz MB, Sun Y, Chen J, Cheng Meng Q, Moore JT, Veasey SC, Dixon S, Thornton M, Funato H, Yanagisawa M. An essential role for orexins in emergence from general anesthesia. *Proc Natl Acad Sci USA*. 2008:105(4):1309–1314.

Konadhode RR, Pelluru D, Blanco-Centurion C, Zayachkivsky A, Liu M, Uhde T, Glen WB Jr, van den Pol AN, Mulholland PJ, Shiromani PJ. Optogenetic stimulation of MCH neurons increases sleep. *J Neurosci*. 2013:33(25):10257–10263.

Koss MC, Gherezghiher T, Nomura A. CNS adrenergic inhibition of parasympathetic oculomotor tone. *J Auton Nerv Syst*. 1984:10(1):55–68.

Kum JE, Han H-B, Choi JH. Pupil Size in Relation to Cortical States during Isoflurane Anesthesia. *Exp Neurobiol*. 2016:25:86–92.

Kringelbach ML, Deco G. Brain states and transitions: insights from computational neuroscience. *Cell Rep*. 2020:32(10):108128.

Lachaux JP, Rodriguez E, Martinerie J, Varela FJ. Measuring phase synchrony in brain signals. *Hum Brain Mapp*. 1999:8(4):194–208.

Lee MG, Hassani OK, Jones BE. Discharge of identified orexin/hypocretin neurons across the sleep-waking cycle. *J Neurosci*. 2005:25(28):6716–6720.

Liu Y, Rodenkirch C, Moskowitz N, Schriver B, Wang Q. Dynamic lateralization of pupil dilation evoked by locus Coeruleus activation results from sympathetic, not parasympathetic. *Contributions Cell Rep*. 2017:20(13):3099–3112.

Lu HB, Zou QH, Gu H, Raichle ME, Stein EA, Yang YH. Rat brains also have a default mode network. *Proc Natl Acad Sci USA*. 2012:109(10):3979–3984.

Magri C, Schridde U, Murayama Y, Panzeri S, Logothetis NK. The amplitude and timing of the BOLD signal reflects the relationship between local field potential power at different frequencies. *J Neurosci*. 2012:32(4):1395–1407.

Marsaglia G, Tsang WW, Wang J. Evaluating Kolmogorov's distribution. *J Stat Softw*. 2003:8(18):1–4.

Mathis A, Mamidanna P, Cury KM, Abe T, Murthy VN, Mathis MW, Bethge M. DeepLabCut: markerless pose estimation of user-defined body parts with deep learning. *Nat Neurosci*. 2018:21(9):1281–1289.

McCormick DA, Nestvogel DB, He BJ. Neuromodulation of brain state and behavior. *Annu Rev Neurosci*. 2020:43(1):391–415.

McGinley MJ, David SV, McCormick DA. Cortical membrane potential signature of optimal states for sensory signal detection. *Neuron*. 2015:87(1):179–192.

Migliorelli C, Bachiller A, Andrade AG, Alonso JF, Mananas MA, Borja C, Gimenez S, Antonijoan RM, Varga AW, Osorio RS, et al. Alterations in EEG connectivity in healthy young adults provide an indicator of sleep depth. *Sleep*. 2019:42(6):zsz081.

Miyamoto D, Hirai D, Fung CC, Inutsuka A, Odagawa M, Suzuki T, Boehringer R, Adaikkan C, Matsubara C, Matsuki N, et al. Top-down cortical input during NREM sleep consolidates perceptual memory. *Science*. 2016:352(6291):1315–1318.

Morgane PJ, Galler JR, Mokler DJ. A review of systems and networks of the limbic forebrain/limbic midbrain. *Prog Neurobiol*. 2005:75(2):143–160.

Mukamel R, Gelbard H, Arieli A, Hasson U, Fried I, Malach R. Coupling between neuronal firing, field potentials, and fMR1 in human auditory cortex. *Science*. 2005:309(5736):951–954.

Mukamel EA, Wong KF, Prerau MJ, Brown EN, Purdon PL. Phase-based measures of cross-frequency coupling in brain electrical dynamics under general anesthesia. *Annu Int Conf IEEE Eng Med Biol Soc*. 2011:2011:1981–1984.

Nair J, Klaassen AL, Poirot J, Vyssotski A, Rasch B, Rainer G. Gamma band directional interactions between basal forebrain and visual cortex during wake and sleep states. *J Physiol-Paris*. 2016:110(1–2):19–28.

Nath T, Mathis A, Chen AC, Patel A, Bethge M, Mathis MW. Using DeepLabCut for 3D markerless pose estimation across species and behaviors. *Nat Protoc*. 2019:14(7):2152–2176.

Nunez PL, Srinivasan R, Westdorp AF, Wijesinghe RS, Tucker DM, Silberstein RB, Cadusch PJ. EEG coherency. I: statistics, reference electrode, volume conduction, Laplacians, cortical imaging, and

interpretation at multiple scales. *Electroencephalogr Clin Neurophysiol*. 1997:103(5):499–515.

Olbrich E, Rusterholz T, LeBourgeois MK, Achermann P. Developmental changes in sleep oscillations during early childhood. *Neural Plast*. 2017:2017:6160959–6160912.

Paasonen J, Stenroos P, Salo RA, Kiviniemi V, Grohn O. Functional connectivity under six anesthesia protocols and the awake condition in rat brain. *NeuroImage*. 2018:172:9–20.

Pagliardini S, Greer JJ, Funk GD, Dickson CT. State-dependent modulation of breathing in urethane-anesthetized rats. *J Neurosci*. 2012:32(33):11259–11270.

Pais-Roldan P, Takahashi K, Sobczak F, Chen Y, Zhao XN, Zeng H, Jiang YY, Yu X. Indexing brain state-dependent pupil dynamics with simultaneous fMRI and optical fiber calcium recording. *Proc Natl Acad Sci USA*. 2020:117(12):6875–6882.

Pal D, Silverstein BH, Sharba L, Li D, Hambrecht-Wiedbusch VS, Hudetz AG, Mashour GA. Propofol, Sevoflurane, and ketamine induce a reversible increase in Delta-gamma and theta-gamma phase-amplitude coupling in frontal cortex of rat. *Front Syst Neurosci*. 2017:11:41.

Paxinos G, Watson C. *The rat brain in stereotaxic coordinates*. 6th ed. Amsterdam: Boston; Academic Press/Elsevier; 2007.

Ranson S, Magoun H. Respiratory and pupillary reactions: induced by electrical stimulation of the hypothalamus. *Arch Neurol Psychiatr*. 1933:29(6):1179–1194.

Reimer J, McGinley MJ, Liu Y, Rodenkirch C, Wang Q, McCormick DA, Tolias AS. Pupil fluctuations track rapid changes in adrenergic and cholinergic activity in cortex. *Nat Commun*. 2016:7(1):13289.

Rodenbeck A, Binder R, Geisler P, Danker-Hopfe H, Lund R, Raschke F, Weeß H-G, Schulz H, Task Force 'Scoring of Polysomnographic Recordings' of the German Sleep S. A review of sleep EEG patterns. Part I: a compilation of amended rules for their visual recognition according to Rechtschaffen and kales. *Somnologie - Schlafforschung und Schlafmedizin*. 2006:10(4):159–175.

Rudebeck PH, Putnam PT, Daniels TE, Yang TM, Mitz AR, Rhodes SEV, Murray EA. A role for primate subgenual cingulate cortex in sustaining autonomic arousal. *Proc Natl Acad Sci USA*. 2014:111(14):5391–5396.

Saper CB, Chou TC, Scammell TE. The sleep switch: hypothalamic control of sleep and wakefulness. *Trends Neurosci*. 2001:24(12):726–731.

Schneider M, Hathway P, Leuchs L, Samann PG, Czisch M, Spoormaker VI. Spontaneous pupil dilations during the resting state are associated with activation of the salience network. *NeuroImage*. 2016:139:189–201.

Scholvinck ML, Maier A, Ye FQ, Duyn JH, Leopold DA. Neural basis of global resting-state fMRI activity. *Proc Natl Acad Sci USA*. 2010:107(22):10238–10243.

Stevens FL, Hurley RA, Taber KH. Anterior cingulate cortex: unique role in cognition and emotion. *J Neuropsychiatry Clin Neurosci*. 2011:23(2):121–125.

Szabadi E. Functional Organization of the Sympathetic Pathways Controlling the pupil: light-inhibited and light-stimulated pathways. *Front Neurol*. 2018:9:1069.

Tagliazucchi E, Laufs H. Decoding wakefulness levels from typical fMRI resting-state data reveals reliable drifts between wakefulness and sleep. *Neuron*. 2014:82(3):695–708.

Tarun A, Wainstein-Andriano D, Sterpenich V, Bayer L, Perogamvros L, Solms M, Axmacher N, Schwartz S, Van De Ville D. NREM sleep stages specifically alter dynamical integration of large-scale brain networks. *iScience*. 2021:24(1):101923.

Tort ABL, Komorowski R, Eichenbaum H, Kopell N. Measuring phase-amplitude coupling between neuronal oscillations of different frequencies. *J Neurophysiol*. 2010:104(2):1195–1210.

Trachsel L, Tobler I, Achermann P, Borbély AA. Sleep continuity and the REM-nonREM cycle in the rat under baseline conditions and after sleep deprivation. *Physiol Behav*. 1991:49(3):575–580.

Turner KL, Gheres KW, Drew PJ. Relating Pupil Diameter and Blinking to Cortical Activity and Hemodynamics across Arousal States. *J Neurosci*. 2023:43:949–964.

Vacas S, Kurien P, Maze M. Sleep and Anesthesia - common mechanisms of action. *Sleep Med Clin*. 2013:8(1):1–9.

Wang MS, He Y, Sejnowski TJ, Yu X. Brain-state dependent astrocytic Ca2+ signals are coupled to both positive and negative BOLD-fMRI signals. *Proc Natl Acad Sci USA*. 2018:115(7):E1647–E1656.

Weber F, Chung S, Beier KT, Xu M, Luo L, Dan Y. Control of REM sleep by ventral medulla GABAergic neurons. *Nature*. 2015:526(7573):435–438.

Whitten TA, Martz LJ, Guico A, Gervais N, Dickson CT. Heat synch: inter- and independence of body-temperature fluctuations and brain-state alternations in urethane-anesthetized rats. *J Neurophysiol*. 2009:102(3):1647–1656.

Wu C, Matias C, Foltynie T, Limousin P, Zrinzo L, Akram H. Dynamic network connectivity reveals markers of response to deep brain stimulation in Parkinson's disease. *Front Hum Neurosci*. 2021:15:729677.

Yellin D, Berkovich-Ohana A, Malach R. Coupling between pupil fluctuations and resting-state fMRI uncovers a slow build-up of antagonistic responses in the human cortex. *NeuroImage*. 2015:106:414–427.

Yin L, Li L, Deng J, Wang D, Guo Y, Zhang X, Li H, Zhao S, Zhong H, Dong H. Optogenetic/Chemogenetic activation of GABAergic neurons in the ventral tegmental area facilitates general Anesthesia via projections to the lateral hypothalamus in mice. *Front Neural Circuits*. 2019:13:73.

Yuzgec O, Prsa M, Zimmermann R, Huber D. Pupil size coupling to cortical states protects the stability of deep sleep via parasympathetic modulation. *Curr Biol*. 2018:28(3):392–400.e3.

Zhou Q, Zhang L, Feng J, Lo CZ. Tracking the main states of dynamic functional connectivity in resting state. *Front Neurosci*. 2019:13:685.